Si(001) Step Dynamics

Chris Pearson, Brian Borovsky, Michael Krueger, Robert Curtis, and Eric Ganz
Department of Physics, University of Minnesota, Minneapolis, Minnesota 55455
(Received 6 October 1994; revised manuscript received 30 December 1994)

We used a scanning tunneling microscope to study the dynamics of step edges on the Si(001)-(2 × 1) reconstructed surface at temperatures from 520 to 700 K. We count changes in step edge position to determine the rates of attachment and detachment events which occur in units of four Si atoms (two dimers). Surface mass transport at these temperatures is dominated by kink diffusion. From an Arrhenius plot we find the effective activation energy for kink diffusion to be 0.97 ± 0.12 eV with a prefactor of 3×10^5 s^{-1}.

PACS numbers: 61.16.Ch, 68.10.Jy, 68.35.Fx, 68.55.–a

As fabrication technology moves to smaller size scales, it is increasingly important to understand the dynamic processes that occur during and after fabrication. The Si(001) surface is the basis for most microfabrication and nanofabrication technologies. Success at this level of fabrication requires a detailed understanding of the surface dynamics during growth. The development of scanning tunneling microscopes (STM) that operate *in situ* at elevated temperatures provides a means with which to study the surface dynamics above room temperature. Growth on the Si(001) surface is controlled by the following competing mechanisms: diffusion of adatoms on terraces, diffusion over step edges, and binding at step edges. This competition produces a surface that has particular electrical, optical, and mechanical properties. A thorough understanding of the surface dynamics is required to control the growth mechanisms which yield the desired properties. In this Letter we study the Si(001)-(2 × 1) reconstructed surface at temperatures from 520 to 700 K in order to further our understanding of the surface dynamics during growth and annealing.

The Si(001) surface has been studied extensively both theoretically and experimentally. However, agreement regarding growth mechanisms and activation energies on this surface has not yet been reached. In a series of elegant STM experiments, Lagally and co-workers studied diffusion [1], step and kink energies [2,3], coarsening during growth [4–6], and motion anisotropy [7] on the Si(001) surface. However, these studies were limited by the need to image the surface at room temperature. More recently, preliminary studies of the Si(001) surface using high temperature STM have been published [8–10]. On the theoretical side, growth models of the Si(001) surface have been developed using first principles [11], molecular dynamics [12,13], and Monte Carlo [14–18] methods. There has also been considerable interest in the relationship between thermal fluctuations in step edge position and surface mass diffusion [19–21]. This has been primarily motivated by the recent ability to observe step fluctuations on the atomic scale [9,10,22–25]. Further experimental results are needed to expand and refine these models.

Our experiment is performed in an ultrahigh vacuum (UHV) chamber with a base pressure of 8×10^{-11} Torr, using a custom built STM. 12.7 mm × 4.8 mm × 0.4 mm samples are cut from Si(001) wafers with 0.1 Ω cm resistivity [26]. Both ends of the samples are wrapped in Ta foil to provide uniform electrical contacts. The samples are cleaned by degassing for several hours at 875 K, followed by repeated cycles of flashing to 1475 K [27]. The samples are finally transferred to the STM stage where they are checked for surface ordering with reflection high energy electron diffraction (RHEED). This process produces a clean Si(001)-(2 × 1) reconstructed surface with approximately 1% total defects. It is known that the Si(001) surface reconstructs to form rows of dimers in order to reduce the number of dangling bonds, with alternate layers exhibiting (2 × 1) and (1 × 2) periodicity. The rows of dimers in each layer terminate either parallel or perpendicular to step edges labeled S_A or S_B, respectively [28]. A typical image of the surface at 520 K showing terraces and dimer rows is shown in Fig. 1.

Unfortunately, direct measurement of sample temperature on the STM stage is difficult in the temperature range of interest. To ensure accurate temperature measurement, we use both an optical pyrometer and a thermocouple to create a plot of sample heating power P versus temperature T. We then use the plot to calculate the temperature from the known sample heating power used during the data runs. The optical pyrometer is used to measure the temperature above 675 K [29]. By calibrating against the Si(111)-(7 × 7) to (1 × 1) phase transition at 1141 K, which we observe simultaneously with RHEED, we estimate an error in the pyrometer measurements of ±3 K. Below 575 K we measure temperature with a type-C thermocouple using the following process. We first press the thermocouple onto the front of the sample. We then retract the thermocouple, heat it to the previously measured temperature, and repeat the process until no change in the thermocouple temperature is observed upon contact with the sample [30]. If the thermocouple is not heated, measurement errors in excess of 30% may occur due to limited thermal contact with the sample. To

 0031-9007/95/74(14)/2710(4)$06.00

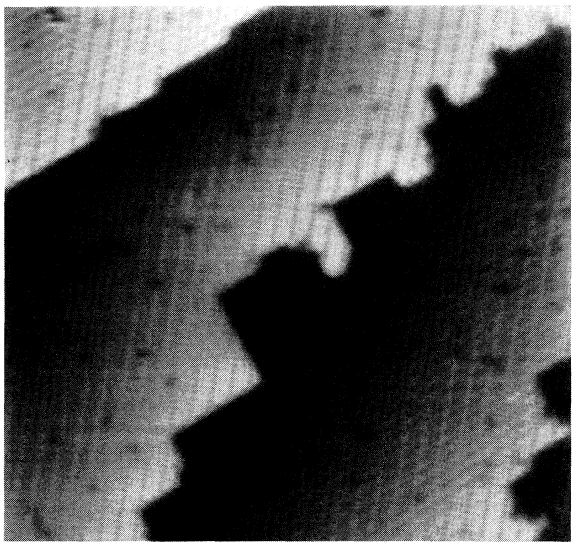

FIG. 1. 400 Å × 400 Å STM image of the Si(001)-(2 × 1) surface at 520 K. The relatively straight type-*A* step is visible at the top left, and the rougher type-*B* step edge runs diagonally across the center of the image.

avoid sample contamination, we make the thermocouple measurements after all STM data runs are finished. We estimate a systematic error of ±10 K for any given thermocouple measurement.

In Fig. 2 we show the results of a temperature calibration. At high temperatures we expect power loss to be dominated by the radiation term $P = A\sigma\varepsilon T^4$, where A is the radiative area, $\sigma = 5.67 \times 10^{-12}$ W/cm^{2}K^4 is the Stefan-Boltzmann constant, and $\varepsilon = 0.68$ is the emissivity of Si. We therefore fit to the curve $P(T) = aT^4 + bT + c$. For the data in Fig. 2, $a = 5.11 \times 10^{-12}$ W/K^4, resulting in an effective radiative area of our sample of 1.3 cm^2. We estimate this process yields an overall accuracy in the temperature measurements of ±7 K. The sample is left in place during all STM imaging and temperature calibration runs to ensure temperature reproducibility.

Figure 3 shows one image from a series of 200 images, each containing four strips, obtained at 682 K. Each strip images the same area of the sample, resulting in a fourfold increase in the observation rate. Within each strip, the lengths of the dimer rows are digitized manually and entered into the computer. Pinned sites, those located next to a dimer vacancy defect, are determined by eye and are not counted. An analysis program counts all initial configurations and the events that occur between subsequent strips. When there is a change in the step configuration, we record the event and the relative positions of the neighboring columns, as observed in the previous strip. In this way we build up statistics on the probability that any possible event will occur given an initial local step configuration. By following the individual microscopic events, we avoid the assumptions and ambiguities of previous studies. We focus on three

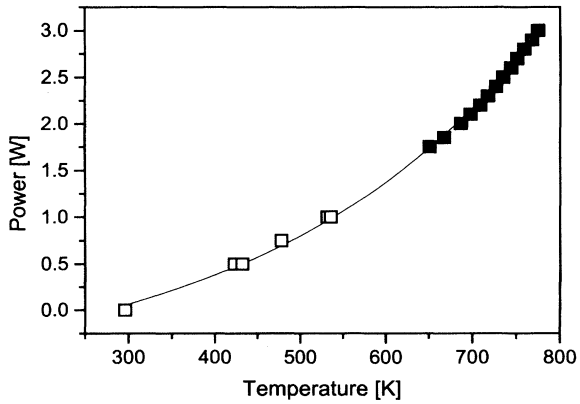

FIG. 2. Temperature calibration for the Si(001) sample used for 682 and 670 K data sets. Empty squares represent thermocouple data and filled squares represent pyrometer data. The solid line is the fit curve $P = 5.112 \times 10^{-12}T^4 + 0.00228T - 0.661$.

important kink events: kink diffusion, kink-antikink annihilation, and kink-antikink creation. These events are diagrammed in Fig. 4. All of these events consist of the attachment or detachment of four atom units at the step edge.

Since kink diffusion is the dominant step edge process, we begin with an analysis of kink diffusion rates. As there is no change in S_A step length for a kink diffusion event, the final state energy difference is small. The observation rate is much faster than the kink diffusion rate, so the probability of multiple events occurring during

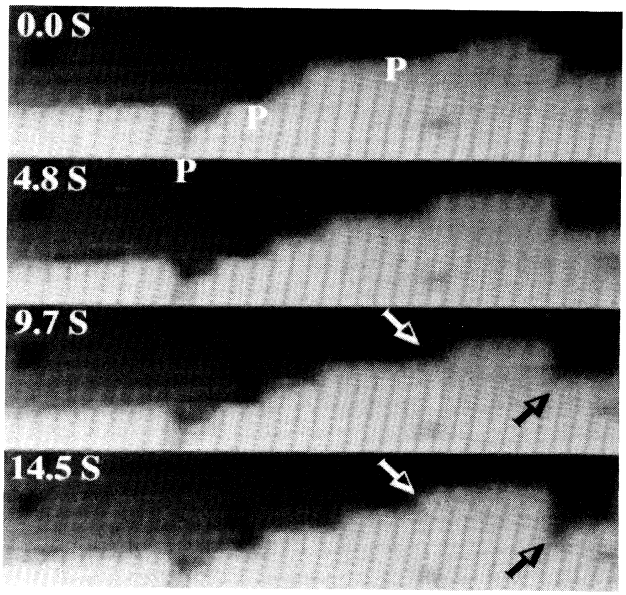

FIG. 3. 220 Å × 220 Å image of the Si(001)-(2 × 1) surface at 682 K. The image is constructed of four subsequent strip images obtained at 4.84 s intervals. We labeled pinned sites with a P. The black arrows identify a kink diffusion event. The white arrows identify an enhanced creation event.

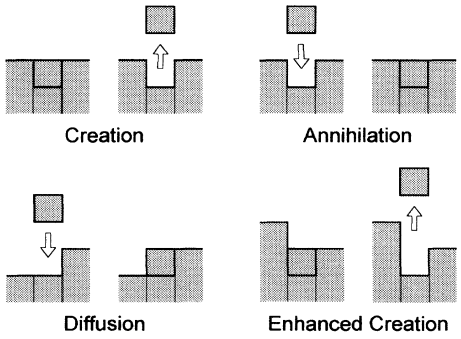

FIG. 4. Schematic diagram showing creation, annihilation, diffusion, and enhanced creation events. Creation events are relatively rare and are usually followed by an annihilation event. Diffusion events are the dominant process on the surface.

our observation time Δt is low. The probability p for an event in an observation time Δt is the number of times an event occurs divided by the number of times an initial configuration is observed. For small p, the event rate is $R \approx p/\Delta t$. We use both right and left kink motion to obtain our result.

Next we consider kink-antikink annihilation and creation rates. For an annihilation event to occur, we must have a starting configuration with a kink-antikink pair, as shown in Fig. 4. Since the kink-antikink creation rate is low and the annihilation rate is high, we see very few events. To amass sufficient statistics, we processed many images; we counted approximately 1200 total events starting from 20 000 configurations (1100 strips analyzed). This produced a total of 53 creation and subsequent annihilation events.

The kink-antikink annihilation events occur on the time scale of image acquisition Δt. Therefore, we must use care in converting the probability of annihilation events given the initial local step configuration (typically $p = 0.3$ to 0.6) to event rates. We assume every strip observation is independent and that the annihilation events occur randomly. After time Δt, the probability that an event has occurred is $p = 1 - e^{-R_a \Delta t}$. The rate for annihilation events to occur is therefore $R_a = -\ln(1 - p)/\Delta t$. For small p this approaches $p/\Delta t$, as in the kink diffusion case above.

Finally, we calculate the kink-antikink creation rate. In this case, the starting configuration (a flat segment of step edge) is quite common and also quite stable. As a result, the probability of creation events given the initial local step configuration is very small, giving an observed creation rate of just $p/\Delta t$. However, when the rare creation event does occur, a rapid annihilation event may heal the edge before the next strip is imaged. To account for this, we multiply the observed creation rate by a correction factor. We assume the creation events occur uniformly during our observation time Δt and decay away at the previously determined annihilation rate R_a, resulting in a correction factor of $R_a \Delta t/(1 - e^{-R_a \Delta t})$. Therefore, $R_c = (p/\Delta t) R_a \Delta t/(1 - e^{-R_a \Delta t})$. A correction factor of 1.6 is found for the 670 and 682 K data sets.

In Fig. 5 we plot the calculated rates for these three events on an Arrhenius plot, because for a thermally activated system we expect $R = \nu e^{-E/k_B T}$. The vertical error bars represent statistical error and the horizontal error bars are due to systematic uncertainty. The kink diffusion line is fit using York's method of fitting data with independent x and y errors, which provides an accurate fit value and error [31]. From the Arrhenius plot we find the effective activation energy for kink diffusion is $E = 0.97 \pm 0.12$ eV, with a prefactor $\nu = 3 \times 10^5\ \mathrm{s}^{-1}$ (range 4×10^4 to $3 \times 10^6\ \mathrm{s}^{-1}$). This activation energy is significantly less than the 1.4–2.0 eV reported earlier [9,10]. We note these earlier energies were computed assuming a prefactor of $10^{13}\ \mathrm{s}^{-1}$, which would be reasonable for a single atom process. Zandvliet, Elswijk, and van Loenen observed a rate of $0.65\ \mathrm{s}^{-1}$ at 725 K, which is consistent with our results [9]. Kitamura *et al.* observed a rate of $0.025\ \mathrm{s}^{-1}$ at 500 K, which is not consistent with our results [10].

We note that the activation energy of 0.97 eV we observe is much lower than the theoretical value for the dimer formation energy of 1.6 eV [16]. This suggests a collective process is involved. The fact that individual dimer motions are not seen presumably reflects the fact that two dimers must leave in order for the uncovered Si atoms on the next terrace to dimerize (upper terrace dimers are perpendicular to the removed dimers). This redimerization energy could thus be recaptured in a collective process, producing a relatively low activation energy. The low effective prefactor of $3 \times 10^5\ \mathrm{s}^{-1}$ also reflects the collective nature of the four atom events [32–34].

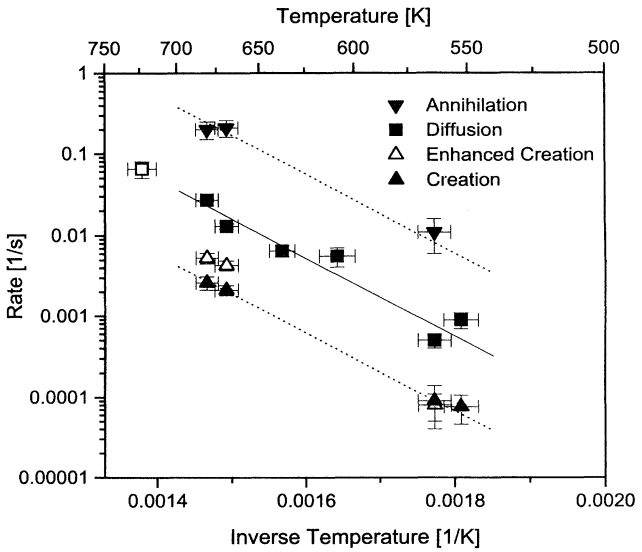

FIG. 5. Arrhenius plot for four kink processes. The solid line corresponds to an activation energy of 0.97 eV and a prefactor of $3 \times 10^5\ \mathrm{s}^{-1}$. The two dotted lines are drawn to guide the eye. We included a value for kink diffusion at 725 K (open square) from Zandvliet, Elswijk, and van Loenen [9].

Surface mass transport is thought to be carried out by monomer motion. In the absence of deposition, monomers are created primarily by escape from kink sites. They diffuse across the surface with an activation energy of 0.67 eV and sample the many configurations and binding sites available [1]. Because escape from kink sites is dominated by kink diffusion, surface mass transport is controlled by kink diffusion.

Prefactors for different kink events reflect the relative stability of the intermediate states that occur along the energy pathway between initial and final state energy. For example, the prefactor for kink-antikink annihilation is high, meaning that once this event has started, completion is very favorable. Local configuration can also affect event rates. For example, we observe significant enhancement of the kink-antikink creation rate at kink sites. The event is shown in Fig. 4 and plotted in Fig. 5 as enhanced creation. We can understand this enhancement by looking closely at the final state energy differences. Swartzentruber *et al.* measured the relationship between kink length and energy and fit the kink energy with a corner term plus a length term $E_k = E_c + 2n\varepsilon_{S_A}$, where n is the kink length [2]. We estimate $E_C = 0.071$ eV and $\varepsilon_{S_A} = 0.032$ eV [35]. To create a kink-antikink pair on a flat area, the final state energy increases by $\Delta E = 2E_c + 4\varepsilon_{S_A}$. However, at a kink site (as in Fig. 4) one of the corners is already created, so the final state energy difference is only $\Delta E = E_c + 4\varepsilon_{S_A}$. This energy difference causes the creation rate to be higher at kink sites. We also observed that kink annihilation is slower at kink sites. This can be understood in the same way, for the energy gained is smaller and thus the rate is lower.

We hope that these careful measurements of Si(001) step edge dynamics will narrow the gap between experiment and theory for this surface. In particular, the semiempirical methods that are used to try to bridge the gap from first principles calculations to experimental growth results require accurate microscopic measurements as reference points [14,16,19].

This research was supported by NSF Grant No. DMR-9222493. We acknowledge Peter Gaard and Xin Shi for programming, our machine shop for fine machining and design suggestions, and Jene Golovchenko and Angus Rockett for helpful discussions.

[1] Y.W. Mo, J. Kleiner, M.B. Webb, and M.G. Lagally, Phys. Rev. Lett. **66**, 1998 (1991); Surf. Sci. **268**, 275 (1992).
[2] B.S. Swartzentruber, Y.W. Mo, R. Kariotis, M.G. Lagally, and M.B. Webb, Phys. Rev. Lett. **65**, 1913 (1990).
[3] B.S. Swartzentruber, N. Kitamura, M.G. Lagally, and M.B. Webb, Phys. Rev. B **47**, 13432 (1993).
[4] M.G. Lagally, R. Kariotis, B.S. Swartzentruber, and Y.W. Mo, Ultramicroscopy **31**, 87 (1989).
[5] Y.W. Mo, B.S. Swartzentruber, R. Kariotis, M.B. Webb, and M.G. Lagally, Phys. Rev. Lett. **63**, 2393 (1989).
[6] Y.W. Mo, R. Kariotis, B.S. Swartzentruber, M.B. Webb, and M.G. Lagally, J. Vac. Sci. Technol. A **8**, 201 (1989).
[7] Y.W. Mo and M.G. Lagally, Surf. Sci. **248**, 313 (1991).
[8] H. Tokumoto and M. Iwatsuki, Jpn. J. Appl. Phys. **32**, 1368 (1993).
[9] H.J.W. Zandvliet, H.B. Elswijk, and E.J. van Loenen, Surf. Sci. **272**, 264 (1992).
[10] N. Kitamura, B.S. Swartzentruber, M.G. Lagally, and M.B. Webb, Phys. Rev. B **48**, 5704 (1993).
[11] G. Brocks, P.J. Kelly, and R. Car, Phys. Rev. Lett. **66**, 1729 (1991).
[12] C. Roland and G.H. Gilmer, Phys. Rev. Lett. **67**, 3188 (1991).
[13] D. Srivastava and B.J. Garrison, Phys. Rev. B **47**, 4464 (1993).
[14] H.B. Elswijk, A.J. Hoeven, E.J. van Loenen, and D. Dijkkamp, J. Vac. Sci. Technol. B **9**, 451 (1991).
[15] Y.T. Lu, Z.Y. Zhang, and H. Metiu, Surf. Sci. **257**, 199 (1991).
[16] A. Rockett, Surf. Sci. **312**, 201 (1994).
[17] C.P. Toh and C.K. Ong, Surf. Sci. Lett. **303**, L348 (1994); **314**, L889 (1994).
[18] H. Spjut and D.A. Faux, Surf. Sci. **306**, 233 (1994).
[19] N.C. Bartelt, T.L. Einstein, and E.D. Williams, Surf. Sci. **312**, 411 (1994).
[20] E.D. Williams, Surf. Sci. **299/300**, 502 (1994).
[21] N.C. Bartelt, R.M. Tromp, and E.D. Williams, Phys. Rev. Lett. **73**, 1656 (1994).
[22] L. Kuipers, M.S. Hoogeman, and J.W.M. Frenken, Phys. Rev. Lett. **71**, 3517 (1993).
[23] M. Giesen-Seibert, R. Jentjens, M. Poensgen, and H. Ibach, Phys. Rev. Lett. **71**, 3521 (1993).
[24] C. Alfonso, J.M. Bermond, J.C. Heyraud, and J.J. Métois, Surf. Sci. **262**, 264 (1991).
[25] N.C. Bartelt, J.L. Goldberg, T.L. Einstein, E.D. Williams, J.C. Heyraud, and J.J. Métois, Phys. Rev. B **48**, 15453 (1993).
[26] The float zone and *P* doped wafers were obtained from Wacker-Chemitronic GmbH.
[27] B.S. Swartzentruber, Y.W. Mo, M.B. Webb, and M.G. Lagally, J. Vac. Sci. Technol. A **7**, 2901 (1989).
[28] D.J. Chadi, Phys. Rev. Lett. **59**, 1691 (1987).
[29] Acufiber model 10 manufactured by Luxtron Corporation.
[30] R.M. Feenstra, A.J. Slavin, G.A. Held, and M.A. Lutz, Ultramicroscopy **42–44**, 33 (1992).
[31] B.C. Reed, Am. J. Phys. **57**, 642 (1989); **58**, 189E (1990).
[32] E. Ganz, S.K. Theiss, I.S. Hwang, and J. Golovchenko, Phys. Rev. Lett. **68**, 1567 (1992).
[33] E. Kaxiras and J. Erlebacher, Phys. Rev. Lett. **72**, 1714 (1994).
[34] N. Kitamura, M.G. Lagally, and M.B. Webb, Phys. Rev. Lett. **71**, 2082 (1993).
[35] C. Pearson, M. Krueger, R. Curtis, B. Borovsky, X. Shi, and E. Ganz (to be published).

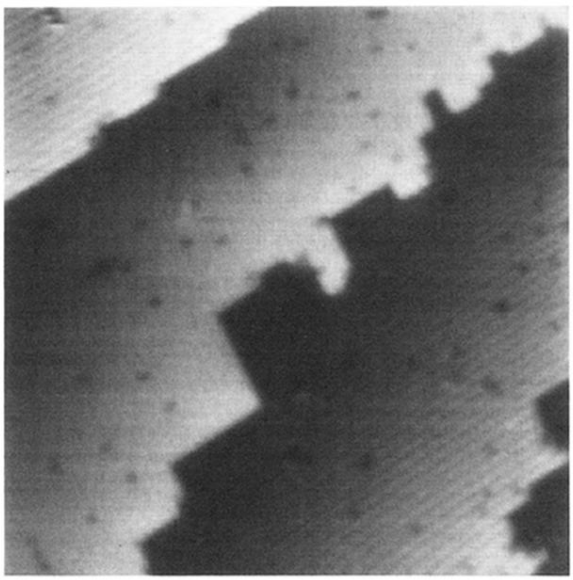

FIG. 1. 400 Å × 400 Å STM image of the Si(001)-(2 × 1) surface at 520 K. The relatively straight type-*A* step is visible at the top left, and the rougher type-*B* step edge runs diagonally across the center of the image.

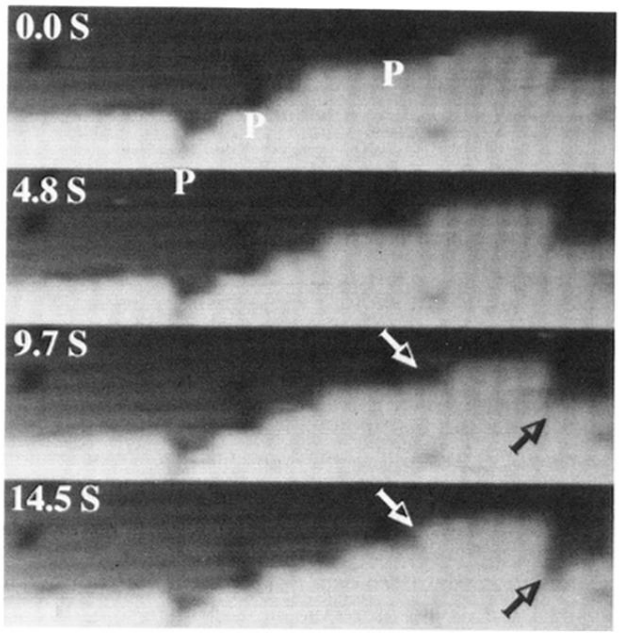

FIG. 3. 220 Å × 220 Å image of the Si(001)-(2 × 1) surface at 682 K. The image is constructed of four subsequent strip images obtained at 4.84 s intervals. We labeled pinned sites with a P. The black arrows identify a kink diffusion event. The white arrows identify an enhanced creation event.